Published online 29 September 2008 *Nucleic Acids Research, 2008, Vol. 36, No. 19* ***6143–6154***
doi:10.1093/nar/gkn612

Nonradioactive, ultrasensitive site-specific protein–protein photocrosslinking: interactions of α-helix 2 of TATA-binding protein with general transcription factor TFIIA and transcriptional repressor NC2

Younggyu Kim[1], Yon W. Ebright[1], Adam R. Goodman[1], Danny Reinberg[2] and Richard H. Ebright[1,*]

[1]Howard Hughes Medical Institute, Waksman Institute, and Department of Chemistry and Chemical Biology, Rutgers University, Piscataway NJ 08854 and [2]Howard Hughes Medical Institute and Department of Biochemistry, New York University Medical School, New York NY 10016, USA

Received August 14, 2008; Revised September 4, 2008; Accepted September 9, 2008

ABSTRACT

We have developed an approach that enables nonradioactive, ultrasensitive (attamole sensitivity) site-specific protein–protein photocrosslinking, and we have applied the approach to the analysis of interactions of α-helix 2 (H2) of human TATA-element binding protein (TBP) with general transcription factor TFIIA and transcriptional repressor NC2. We have found that TBP H2 can be crosslinked to TFIIA in the TFIIA–TBP–DNA complex and in higher order transcription–initiation complexes, and we have mapped the crosslink to the 'connector' region of the TFIIA α/β subunit (TFIIAα/β). We further have found that TBP H2 can be crosslinked to NC2 in the NC2–TBP–DNA complex, and we have mapped the crosslink to the C-terminal 'tail' of the NC2 α-subunit (NC2α). Interactions of TBP H2 with the TFIIAα/β connector and the NC2α C-terminal tail were not observed in crystal structures of TFIIA–TBP–DNA and NC2–TBP–DNA complexes, since relevant segments of TFIIA and NC2 were not present in truncated TFIIA and NC2 derivatives used for crystallization. We propose that interactions of TBP H2 with the TFIIAα/β connector and the NC2α C-terminal tail provide an explanation for genetic results suggesting importance of TBP H2 in TBP–TFIIA interactions and TBP–NC2 interactions, and provide an explanation—steric exclusion—for competition between TFIIA and NC2.

INTRODUCTION

This work provides evidence for interactions of α-helix 2 (H2) of human TATA-element binding protein (TBP) with the human general transcription factor TFIIA and with the human transcriptional repressor NC2.

TBP is the critical functional subunit of the eukaryotic general transcription factor TFIID (1–4). In transcription initiation at a eukaryotic protein-encoding gene, TBP binds to the TATA element, bends the TATA element and nucleates assembly of general transcription factors and RNA polymerase II (RNAPII) to yield a transcription initiation complex. Human TBP has a molecular mass of 37 kDa and consists of a nonconserved, unstructured N-terminal domain (TBPn) and a conserved, structured C-terminal domain (TBPc). Human TBPc contains all determinants required for DNA binding, DNA bending and transcription–initiation-complex assembly.

The eukaryotic general transcription factor TFIIA facilitates formation of stable TBP–DNA complexes and higher order transcription–initiation complexes (1–5). TFIIA functions by binding to TBP–DNA complexes and higher order transcription–initiation complexes, making protein–protein interactions with TBP and

*To whom correspondence should be addressed. Tel: 732 445 5179; Fax: 732 445 5735; Email: ebright@waksman.rutgers.edu
Correspondence may also be addressed to Danny Reinberg. Tel: 212 263 9036; Fax: 212 263 9040; Email: reinbd01@med.nyu.edu
Present addresses:
Younggyu Kim, Department of Chemistry and Biochemistry, University of California, Los Angeles, CA 90095, USA.
Adam Goodman, Northwest Biomedical Research and Consulting, West Linn, OR 97068, USA.

The authors wish it to be known that, in their opinion, the first two authors should be regarded as joint First Authors.

making protein–DNA interactions with DNA adjacent to the TATA element. TFIIA is able to mediate responses to transcriptional activators; in this role, TFIIA is recruited by transcriptional activators to specific target promoters, where it facilitates formation of stable TBP–DNA and higher order transcription–initiation complexes. Human TFIIA has a molecular mass of 53 kDa and consists of one TFIIAα/β subunit (or its proteolytic-cleavage products, TFIIAα and TFIIAβ) and one TFIIAγ subunit.

The eukaryotic transcriptional repressor NC2 (also known as Drap1/Dr1) inhibits formation of transcription–initiation complexes (6,7). Human NC2 functions by inhibiting two sets of interactions: (i) interactions between the general transcription factor TFIIA and TBP and (ii) interactions between the general transcription factor TFIIB and TBP. Human NC2 has a molecular mass of 42 kDa and consists of one NC2α subunit (also known as Drap1) and one NC2β subunit (also known as Dr1).

Full structural descriptions of TFIIA–TBP interactions and of NC2–TBP interactions have remained elusive, and, as a result, an understanding of the structural basis of competition between TFIIA and NC2 has remained elusive.

Four crystal structures of TFIIA–TBP–DNA complexes have been reported (8–10). One set of expected, genetically defined, TFIIA–TBP interactions, involving TBP β-strand 2 (11), is observed in the four crystal structures (8–10). However, a second set of expected, genetically and spectroscopically defined, TFIIA–TBP interactions, involving TBP α-helix 2 (H2; 12–17), is not observed—or is observed only equivocally and in part—in the four crystal structures (8–10). A large segment of TFIIA, comprising >100 amino acids in the 'connector' segment of the TFIIAα/β subunit of TFIIA, was omitted from the polypeptides used for crystallization for the four crystal structures. This omission may account for the failure to observe the second set of expected TFIIA–TBP interactions.

One crystal structure of an NC2–TBP–DNA complex has been reported (7). One set of expected, genetically defined, NC2–TBP interactions, involving the loop between TBP α-helix 2′ and β-strands 2′–4′ (16), is observed in the crystal structure (7). However, a second set of expected, genetically defined, NC2–TBP interactions, involving TBP H2 (18), is not observed in the crystal structure (7). The crystal structure provides a clear basis for observed competition between NC2 and TFIIB (with overlap, and steric clash, between observed positions of residues of NC2 that interact with TBP and observed positions of residues of TFIIB that interact with TBP). However, the crystal structure does not provide a clear basis for observed competition between NC2 and TFIIA (with minimal overlap, and minimal steric incompatibility, between observed positions of residues of NC2 that interact with TBP and residues of TFIIA that interact with TBP). A large segment of NC2α, comprising the C-terminal 'tail' of NC2α, was omitted from the polypeptide used for crystallization. This omission may account for the failure to observe the second set of expected NC2–TBP interactions and for the failure to provide a clear basis for competition between NC2 and TFIIA.

In this work, to provide a more complete description of TFIIA–TBP and NC2–TBP interactions—and, in particular, to define possible interactions involving TBP H2 and possible interactions involving TFIIA and NC2 determinants omitted from polypeptides used for crystallization—we have performed site-specific protein–protein photocrosslinking (19,20). To facilitate the work and to enable the extension of the work to higher order transcription-initiation complexes that can be produced in only limited quantities, we have developed novel reagents and procedures for nonradioactive, ultrasensitive (attamole sensitivity) site-specific protein–protein photocrosslinking.

EXPERIMENTAL PROCEDURES

(2-((*N*-biotinyl-2-aminoethyl)carbamoyl)-2′-tritylamino-ethylthio)-triphenylmethane (I)

Biotin ethylenediamine HBr (Invitrogen, Inc., Carlsbad, CA, USA; 100 mg; 0.27 mmol) was added to a solution of *N*-(*N*-trityl-*S*-trityl-L-cysteinyloxy)succinimide (Novabiochem, Inc., Gibbstown, NJ, USA; 190 mg; 0.24 mmol,) in 10 ml anhydrous dimethylformamide and 80 μl triethylamine, and the sample was stirred overnight at room temperature under argon. The sample was evaporated to a viscous oil, redissolved in 10 ml chloroform, extracted with 10 ml 5% sodium bicarbonate, extracted with 10 ml brine, dried over anhydrous sodium sulfate and evaporated to a foamy white solid. Yield: 186 mg (0.21 mmol; 89% yield). $(M+H^+)$: calculated, 874; found, 874.

(2-((*N*-biotinyl-2-aminoethyl)carbamoyl)-2′-(4-azidosalicylamido)-ethylthio)-triphenylmethane (II)

Trifluoroacetic acid (Aldrich Inc., St. Louis, MO, USA; 200 μl) was added to a solution of **I** (168 mg; 0.192 mmol) in 3 ml chloroform. The resulting yellow solution was mixed well and was allowed to react for 10 min. Methanol was then added until the yellow color disappeared. The sample was evaporated to an oil and partly purified by silica flash chromatography (240–400 mesh; 10–20% methanol in chloroform) to afford (2-((*N*-biotinyl-2-aminoethyl)carbamoyl)-2′-amino-ethylthio)-triphenylmethane. Yield: 150 mg white powder (0.24 mmol; >100% crude yield). $(M+H^+)$: calculated, 632; found, 632. The resulting material (150 mg; 0.24 mmol; dissolved in 3 ml DMF and 54 μl triethylamine) was added to *N*-hydroxysuccinimidyl-4-azidosalicylic acid (Aldrich, Inc.; 50 mg; 0.018 mmol; dissolved in 1 ml dimethylformamide) and the sample was stirred overnight at room temperature under argon. Methanol (1 ml) was added to quench the reaction, and the sample was evaporated to a viscous oil, redissolved in 10 ml chloroform, extracted with 10 ml 5% sodium bicarbonate, extracted with 10 ml brine, dried over anhydrous sodium sulfate and concentrated to a viscous oil. The product was purified by silica flash chromatography (10% methanol in chloroform). Yield: 76 mg (0.096 mmol; 53% yield). $(M+H^+)$: calculated, 793; found, 793.

S-(2-((N-biotinyl-2-aminoethyl)carbamoyl)-2′-(4-azidosalicylamido)-ethylthio)-2-thiopyridine (III; B-AET)

Trifluoroacetic acid (Aldrich, Inc.; 1 ml) and triethylsilane (Aldrich, Inc.; 100 µl; 0.626 mmol) were added to a solution of **II** (60 mg; 0.075 mmol) in 1 ml dichloromethane. The yellow solution was mixed well for 5 min and then evaporated to a white powder. The sample was triturated with 2 ml cold methanol, redissolved in chloroform and purified by flash chromatography (15% MeOH in $CHCl_3$.) to afford 2-((*N*-biotinyl-2-aminoethyl)carbamoyl)-2′-(4-azidosalicylamido)-ethyl sulfide. Yield: 33 mg white solid (0.061 mmol; 81% yield). $(M+H^+)$: calculated, 551; found, 551. The resulting material (28 mg; 0.05 mmol; dissolved in 2 ml methanol and 400 µl acetic acid) was added, in 200 µl aliquots over 20 min, to 2,2′-dithiodipyridine (Aldrich, Inc.; 55 mg; 0.25 mmol; dissolved in 2 ml methanol and 80 µl acetic acid). The sample was evaporated to a yellow oil, triturated with diethyl ether, redissolved in chloroform and purified by repeated cycles of preparative thin-layer chromatography on silica gel (Analtech, Inc., Newark, DE, USA; 1000 µm; 10% methanol in chloroform). (Repeated cycles of preparative thin-layer chromatography were needed to eliminate all traces of 2-thiopyridine.) Yield: 8 mg white solid (0.012 mmol; 24% yield). $(M+H^+)$: calculated, 661; found, 661.

(2-((N-biotinyl-11-amino-3,6,9-trioxaundecanyl)-carbamoyl)-2′-tritylamino-ethylthio)-triphenylmethane (IV)

(+)-Biotinyl-3,6,9-trioxaundecanediamine (Pierce, Inc., Rockford, IL, USA; 50 mg; 0.12 mmol) in 300 µl anhydrous dimethylformamide was added to a solution of *N*-(*N*-trityl-*S*-trityl-L-cysteinyloxy)succinimide (Novabiochem, Inc.; 84 mg; 0.12 mmol) in 300 µl anhydrous dimethylformamide and 20 µl triethylamine, and the sample was stirred overnight at room temperature under argon. The sample was evaporated to a viscous oil, redissolved in 4 ml chloroform, extracted with 4 ml 5% sodium bicarbonate, extracted with 4 ml brine, dried over anhydrous sodium sulfate and evaporated to a creamy white solid. Yield: 114 mg (0.115 mmol; 96% yield). $(M+H^+)$: calculated, 993; found, 993.

(2-((N-biotinyl-11-amino-3,6,9-trioxaundecanyl)-carbamoyl)-2′-(4-azidosalicylamido)-ethylthio)-triphenylmethane (V)

Trifluoroacetic acid (Aldrich, Inc.; 200 µl) was added to a solution of **IV** (90 mg; 0.091 mmol) in 3 ml chloroform. The resulting yellow solution was mixed well and was allowed to react for 10 min. Methanol then was added until the yellow color disappeared. The sample was evaporated to an oil and purified by silica flash chromatography (240–400 mesh; 10% methanol in chloroform) to afford (2-((*N*-biotinyl-11-amino-3,6,9-trioxaundecanyl) carbamoyl)-2′-amino-ethylthio)-triphenylmethane. Yield: 51 mg white solid (0.068 mmol; 75% yield). $(M+H^+)$: calculated, 750; found, 750. The resulting material (51 mg; 0.068 mmol; dissolved in 2 ml dimethylformamide and 20 µl triethylamine) was added to *N*-hydroxysuccinimidyl-4-azidosalicylic acid (Aldrich, Inc.; 20 mg; 0.072 mmol; dissolved in 1 ml dimethylformamide), and the sample was stirred overnight at room temperature under argon. Methanol (1 ml) was added to quench the reaction, and the sample was then evaporated to a viscous oil, redissolved in 5 ml chloroform, extracted with 5 ml 5% sodium bicarbonate, extracted with 5 ml brine, dried over anhydrous sodium sulfate, concentrated to a viscous oil and purified by silica flash chromatography (10% methanol in chloroform). Yield: 27 mg (0.030 mmol; 42% yield). $(M+H^+)$: calculated, 911; found, 911.

S-(2-((N-biotinyl-11-amino-3,6,9-trioxaundecanyl)carbamoyl)-2′-(4-azidosalicylamido)-ethylthio)-2-thiopyridine (VI; B-TEG-AET)

Trifluoroacetic acid (Aldrich, Inc.; 500 µl) and triethylsilane (Aldrich, Inc.; 50 µl; 0.318 mmol) were added to a solution of **V** (27 mg; 0.030 mmol) in 0.5 ml dichloromethane. The yellow solution was mixed well for 10 min and then evaporated to a white powder. The sample was triturated with 1 ml cold methanol, redissolved in chloroform and purified by flash chromatography (10% methanol in chloroform.) to afford (2-((*N*-biotinyl-11-amino-3,6,9-trioxaundecanyl)carbamoyl)-2′-(4-azidosalicylamido)-ethyl sulfide. Yield: 16.4 mg white solid (0.025 mmol; 83% yield). $(M+H^+)$: calculated, 669; found, 669. The resulting material (16 mg, 0.025 mmol; dissolved in 1 ml methanol and 200 µl acetic acid) was added, in 50 µl aliquots over 20 min, to 2,2′-dithiodipyridine (Aldrich, Inc.; 30 mg; 0.136 mmol; dissolved in 1 ml methanol and 50 µl acetic acid). The sample was evaporated to a yellow oil, triturated with diethyl ether, redissolved in chloroform and purified by repeated cycles of preparative thin-layer chromatography in silica gel (Analtech, Inc.; 250 µm; 10% methanol in chloroform). Yield: 8.5 mg white solid (0.011 mmol; 44% yield). $(M+H^+)$: calculated, 778; found, 778.

DNA fragments

DNA fragment AdMLP(−50/−16) contains positions −50 to −16 of the adenovirus major late promoter. DNA fragment AdMLP(−50/−16)-NH2 contains positions −50 to −16 of the adenovirus major late promoter and also contains a bottom-strand 5′-terminal C6 amino link. DNA fragments were prepared by total synthesis.

DNA agarose

AdMLP(−50/−16)-agarose was prepared by reaction of DNA fragment AdMLP(−50/−16)-NH_2 (60 pmol or 2 nmol in 0.1 M sodium carbonate, pH 8.6) with Affiprep15 Agarose (BioRad, Inc., Hercules, CA, USA; 1 ml) per instructions of the manufacturer, was washed with TE (20 mM Tris–HCl, pH 8.0 and 1 mM EDTA) and was stored in TE at 4°C. The incorporation efficiency was ∼50% (i.e. ∼30 pmol or ∼1 nmol DNA fragment incorporated per milliliter agarose).

TBPc derivatives

Plasmid pHTT7f1-NH-TBPc encodes N-terminally hexahistidine-tagged human TBPc under control of the bacteriophage gene 10 promoter and the *lac* operator (15). Derivatives of plasmid pHTT7f1-NH-TBPc encoding N-terminally hexahistidine-tagged [Thr176]TBPc and [Thr176;Cys236]TBPc were constructed using site-directed mutagenesis (21). TBPc derivatives were overproduced in transformants of *Escherichia coli* strain BL21(DE3) (Novagen, Inc., Madison, WI, USA); purified under native conditions by metal-ion affinity chromatography on Ni^{2+}-NTA-agarose [Qiagen, Inc., Valencia, CA, USA; loading in buffer A (20 mM Tris–HCl, pH 7.9, 500 mM NaCl and 1 mM β-mercaptoethanol) containing 5 mM imidazole; washing with buffer A containing 5 mM imidazole and buffer A containing 50 mM imidazole; and elution with buffer A containing 150 mM imidazole]; desalted into buffer B (20 mM Tris–HCl, pH 7.9, 500 mM KCl, 0.1 mM EDTA and 15% glycerol) on Bio-Gel P-6DG (BioRad, Inc.); concentrated using collodion membranes (Schleicher & Schuell, Inc., Dassel, Germany; 10 K MWCO); and stored in aliquots at −80°C. Typically, the yield was 2–3 mg TBPc derivative per liter of bacterial culture. Quantitation of solvent-accessible cysteine was performed by a modification of the procedure of Ref. (22). Reactions contained (500 μl): 2 μM TBPc derivative, 0.1 mM 5,5′-dithiobis(2-nitrobenzoate) (Aldrich, Inc.), 20 mM Tris–HCl, pH 8.0, 200 mM KCl and 5% glycerol. Formation of 5-thio-2-nitrobenzoate anion was estimated from absorbance at 412 nm after reaction for 15 min (ε_{412} = 13 600 $M^{-1}\,cm^{-1}$).

Labeled TBPc derivatives

Reaction mixtures contained (400 μl): 300 μM TBPc derivative [subjected to solid-phase reduction on Reduce-Imm (Pierce, Inc.) per instructions of the manufacturer immediately before use], 300 μM B-AET or B-TEG-AET, 100 mM sodium phosphate, pH 8.0, 1 mM EDTA and 5% dimethylsulfoxide. Following 20 min at 22°C samples were applied to a NAP-10 desalting column (GE Healthcare Life Sciences, Inc., Piscataway, NJ, USA) pre-equilibrated in buffer B and were eluted in buffer B. Samples were concentrated and dialyzed against buffer C (20 mM Tris–HCl, pH 7.9, 100 mM KCl, 0.1 mM EDTA and 15% glycerol) using collodion membranes (Schleicher & Schuell, Inc.; 10 K MWCO) and were stored in aliquots at −80°C. Labeling efficiencies and labeling specificities were determined spectrophotometrically (using ε_{278} = 10,887 $M^{-1}\,cm^{-1}$ and ε_{330} = 0 $M^{-1}\,cm^{-1}$ for the protein; and using ε_{278} = 2000 $M^{-1}\,cm^{-1}$, ε_{330} = 4576 $M^{-1}\,cm^{-1}$ for the probe). Labeling efficiencies also were determined by quantitation of solvent-accessible cysteine (methods as in preceding paragraph).

TFIIA derivatives

Plasmids pQTFIIA-αβ and pQTFIIA-γ encode N-terminally hexahistidine-tagged human TFIIAα/β and N-terminally hexahistidine-tagged human TFIIAγ under control of a bacteriophage T5 promoter and *lac* operator (23). Derivatives of plasmid pQTFIIA-αβ encoding N-terminally hexahistidine-tagged [Ala337]TFIIAα/β, [Cys61;Ala337]TFIIAα/β, [Cys80;Ala337]TFIIAα/β, [Cys95;Ala337]TFIIAα/β, [Cys110;Ala337]TFIIAα/β, [Cys135;Ala337]TFIIAα/β and [Cys214;Ala337]TFIIAα/β were constructed using site-directed mutagenesis (21). TFIIAα/β derivatives and TFIIγ derivatives were overproduced in transformants of *E. coli* strain M15(pREP4) (Invitrogen, Inc.) TFIIAα/β derivatives and TFIIγ derivatives were purified, and TFIIA derivatives were reconstituted, by the procedures of Ref. (23). The resulting TFIIA derivatives were dialyzed against buffer D (25 mM Tris–HCl, pH 7.9, 500 mM KCl, 0.1 mM EDTA and 10% glycerol); concentrated using collodion membranes (Schleicher & Schuell, Inc.; 25 K MWCO); further purified by gel filtration on Superdex 200 10/30 (GE Healthcare, Inc.); desalted into buffer E (25 mM Tris–HCl, pH 7.9, 100 mM KCl, 0.1 mM EDTA and 10% glycerol) on Bio-Gel P-6DG (BioRad, Inc.) and stored in aliquots at −80°C.

NC2 derivatives

Plasmids pET15b-DRAP1 and pET-NH-DR1 encode N-terminally hexahistidine-tagged human NC2α and N-terminally hexahistidine-tagged human NC2β under control of the bacteriophage gene 10 promoter and the *lac* operator (24,25). A derivative of plasmid pET15b-DRAP1 encoding N-terminally hexahistidine-tagged [Ser54]NC2α was constructed using site-directed mutagenesis (21). NC2α derivatives and NC2β derivatives were overproduced in transformants of *E. coli* strain BL21(DE3) (Novagen, Inc.), and were purified under denaturing conditions by metal-ion affinity chromatography on Ni^{2+}NTA-agarose [Qiagen, Inc.; pH-shift elution; procedures per instructions of the manufacturer]. NC2 derivatives were reconstituted by addition of 3 mg (100 nmol) NC2α derivative to 2 mg (100 nmol) NC2β derivative in 100 mM sodium phosphate, pH 4.5, 10 mM Tris–HCl and 8 M urea; dilution of the sample to 0.5 mg/ml with 100 mM sodium phosphate, 10 mM Tris–HCl, pH 8.0 and 8 M urea; stepwise dialysis, with 6–12 h per step, against buffer E containing 2 M urea, against buffer E containing 0.5 M urea and against buffer E; concentration using a collodion membrane (Schleicher & Schuell, Inc.; 25 K MWCO); and further purification by gel filtration on Superdex 200 HiLoad 16/60 (GE Healthcare, Inc.) pre-equilibrated with, and eluted with, buffer D; and were stored in aliquots at −80°C.

TFIIB

Human TFIIB was prepared as in Ref. (26) (except that the wash buffer in metal-ion affinity chromatography contained 45 mM imidazole), desalted into buffer E on Bio-Gel P-6DG (Bio-Rad, Inc.) and stored in aliquots at −80°C.

TFIIF

Human TFIIF was prepared as in Ref. (26), desalted into buffer D on Bio-Gel P-6DG (BioRad, Inc.) and stored in aliquots at −80°C.

RNAPII

Human RNAPII was prepared as in Ref. (26), dialyzed against buffer E containing 10 mM β-mercaptoethanol and 40% glycerol and stored in aliquots at −80°C.

Electrophoretic-mobility shift assays

Electrophoretic mobility shift assays were performed as in Ref. (15), except that the DNA fragment was AdMLP(−60/−15).

Avidin–biotin-complex blotting

Proteins were separated by SDS–PAGE and were transferred to PVDF membranes (Immobilon-P; Millipore, Inc.) in transfer buffer (25 mM Tris base, 200 mM glycine and 20% methanol) for 1 h at 4°C at 100 V in a Mini Trans-Blot electrophoretic-transfer cell (Bio-Rad, Inc.). Membranes were incubated for at least 10 min at 22°C in PBS (5 mM sodium phosphate, pH 7.2 and 150 mM NaCl) containing 0.2% Tween-20 (Pierce, Inc.) and then were incubated for at least 1 h at 22°C in blocking solution [PBS containing 6% casein (Tropix, Inc., Bedford, MA, USA) and 0.1% Tween-20; prepared by gently stirring PBS containing 6% casein for 1 h at 65°C, followed by cooling to 22°C, followed by addition of Tween-20; stripped of contaminating of biotin and biotinylated proteins by incubation for 16 h at 4°C with 0.01 volume of avidin-agarose (Sigma, Inc.); filtered through a sintered-glass filter; and stored at −20°C]. Blocked membranes were washed for 10 min at 22°C with Avidin–biotin complex (ABC) wash buffer (PBS containing 0.1% casein and Tween-20), were incubated for 30 min at 22°C with gentle agitation in Vecstain Elite ABC agent (Vector Laboratories, Inc., Burlingame, CA, USA; prepared during the blocking step by addition of 45 µl Vecstain Elite ABC agent A and 45 µl Vecstain Elite ABC agent B to 2.5 ml ABC wash buffer and incubation for 30 min at 22°C, followed by addition of 20 ml blocking buffer at 22°C), and were repeatedly washed with ABC wash buffer at 22°C (at least 10 changes of wash buffer over 3–4 h). Processed membranes were applied to SuperSignal West Femto Maximum Sensitivity Substrate (Pierce, Inc.), incubated for 3 min at 22°C, and placed in a development folder (Tropix, Inc.) with BioMax ML film (Kodak, Inc., Rochester, NY, USA). Detection sensitivities were quantified by performing dilution series with a preparation of biotinylated bovine serum albumin containing 13-mol biotin per mole protein (Sigma, Inc.).

Ni^{2+}-NTA-conjugated horseradish peroxidase blotting

Ni^{2+}-NTA-conjugated horseradish peroxidase blotting was performed using Ni-NTA-conjugated HRP (Qiagen, Inc.; procedures per instructions of the manufacturer) and SuperSignal West Femto Maximum Sensitivity Substrate (Pierce, Inc.).

Photocrosslinking

Standard reaction mixtures contained (50 µl): 30 nM [Thr176;(B-AE)Cys236]TBPc or [Thr176;(B-TEG-AE) Cys236]TBPc and 150 fmol DNA fragment AdMLP (−50/−16) immobilized on agarose beads [0.005 ml AdMLP(−50/−16)-agarose containing 30 pmol DNA per milliliter agarose], in buffer F [20 mM Tris–HCl, 20 mM HEPES–NaOH, pH 7.9, 60 mM KCl, 10 mM $MgCl_2$, 8 mM $(NH_4)_2SO_4$, 0.05 mM EDTA, 0.1 mM phenylmethylsulfonyl fluoride, 25 µg/ml poly(dG-dC) (GE Healthcare, Inc; mean size, 700 kDa), 24 mg/ml polyethylene glycol (mean size, 8 kDa) and 5% glycerol]. For experiments with the TFIIA–TBP–DNA complex, TFIIA derivatives were added to standard reaction mixtures to a final concentration of 200 nM. For experiments with the NC2–TBP–DNA complex, NC2 derivatives were added to standard reaction mixtures to a final concentration of 200 nM. For experiments with the RNAPII–TFIIF–TFIIB–TFIIA–TBP–DNA complex, RNAPII, TFIIF, TFIIB, TFIIA and 2-mercaptoethanol were added to standard reaction mixture to final concentrations of 100 nM, 100 nM, 60 nM, 60 nM and 1 mM, respectively. Reaction mixtures were incubated for 30 min at 30°C with gentle agitation, and then were transferred to polystyrene microcentrifuge tubes. Complexes immobilized on agarose beads were collected by centrifugation (2000*g*; 2 min at 22°C), washed twice with 200 µl of buffer UV-irradiated for 20 s at 350 nm at 1×10^5 erg mm^{-2} s^{-2} in a Rayonet RPR100 photochemical reactor (Southern New England Ultraviolet, Inc., Branford, CT, USA).

Crosslink detection

Immediately following UV-irradiation, crosslink-cleavage/label-transfer solution (30 µl, 1.5 M urea, 150 mM sodium iodide and 150 mM 2-mercaptoethanol) was added, and samples were incubated for 15 min at 22°C. Samples were clarified by centrifugation (2000*g*; 2 min at 22°C), transferred to new tubes, mixed with SDS–PAGE loading buffer (27) and analyzed by SDS–PAGE (precast gradient gels; Invitrogen, Inc.) followed by ABC blotting.

Crosslink mapping

Large-scale crosslinking reactions for crosslink mapping were performed as described above for standard crosslinking reactions, except that the reaction volume was 1 ml and the reaction contained 10 pmol DNA fragment AdMLP(−50/−16) immobilized on agarose beads [0.01 ml AdMLP(−50/−16)-agarose containing 1 nmol DNA per milliliter agarose]. Following cross-link cleavage, label transfer and SDS–PAGE (performed as described above for standard crosslinking reactions), gel slices containing proteins of interest were excised, washed four times with 1 ml water and crushed using a microcentrifuge pestle. Proteins were eluted by incubation of crushed gel slices in 3 volumes of 0.1% SDS and 5 mM 2-mercaptoethanol for 12 h at 22°C with gentle agitation and were precipitated by addition of ice-cold acetone (28,29). Proteins were redissolved in 20 µl 0.2 M Tris–HCl, pH 8.3, 0.1% SDS and 5 mM *tris*(2-carboxyethylphosphine)-hydrochloride (Pierce, Inc.); incubated for 15 min at 65°C; incubated for 15 min at 37°C; supplemented with 2 µl 0.15 M 2-nitro-5-thiocyanatobenzoic acid (Aldrich, Inc.; dissolved in ethanol); incubated for

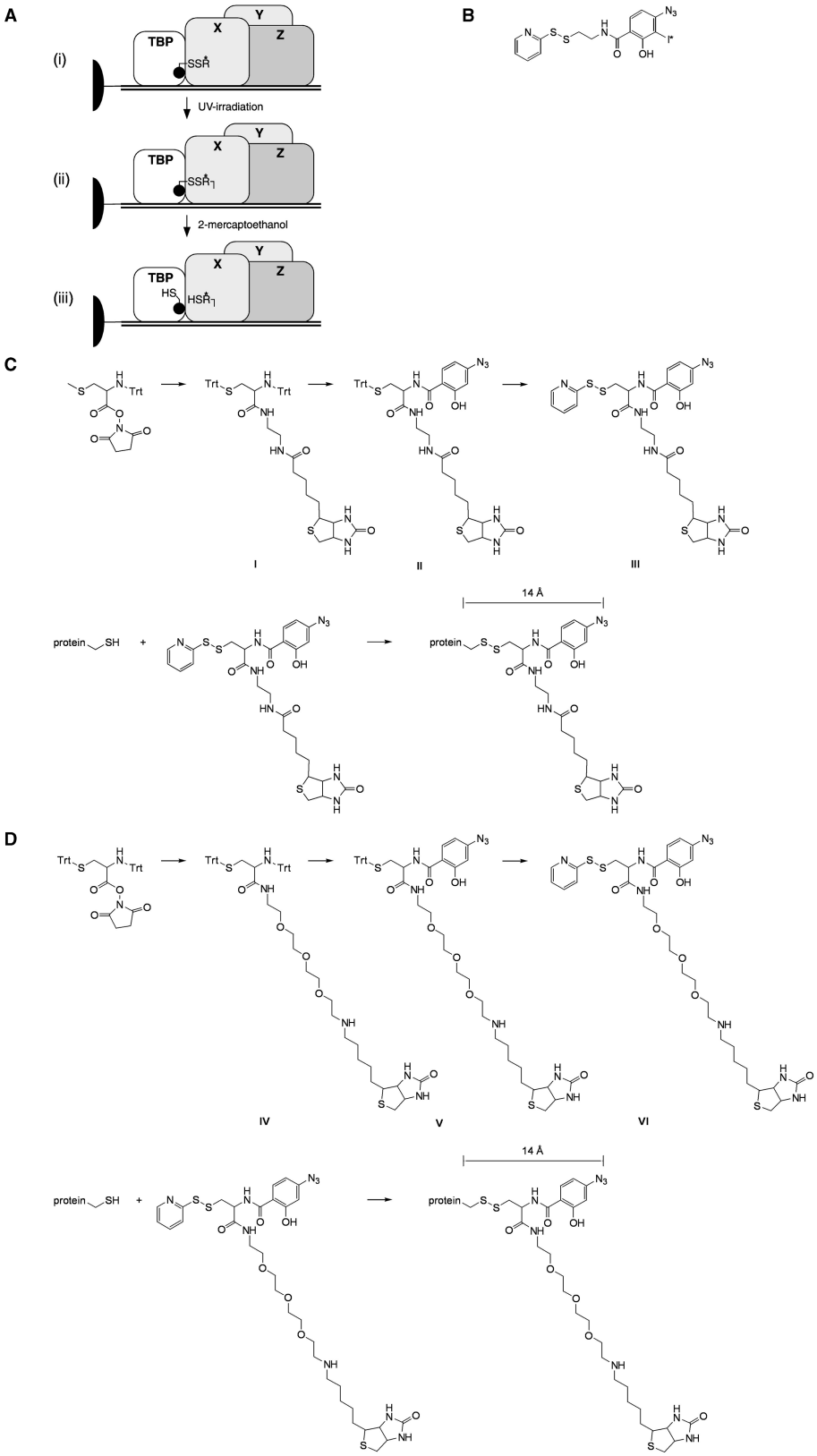

Figure 1. Site-specific protein–protein photocrosslinking. (**A**) Strategy for identification of protein(s) and amino acid(s) close to a single, defined site of interest within a multiprotein complex by use of photocrosslinking and label transfer (19,20). (i) Formation of a multiprotein complex having a photoactivatible crosslinking agent incorporated at a single, defined site of interest. The photoactivatible crosslinking agent contains a detectable label (asterisk) and is attached to the site of interest through a disulfide linker (SS). (ii) Photocrosslinking. (iii) Cleavage and label transfer. (**B**) ^{125}I-AET [photocrosslinking agent of previous work; also known as ^{125}I-PEAS; detectable label is ^{125}I; (19,20)]. (**C**) B-AET

15 min at 37°C; supplemented with 1.5–1.7 µl 1 M NaOH to adjust pH to 9.0; and incubated for 16 h at 37°C with a mineral oil overlay. Cleavage products were analyzed by SDS–PAGE followed by ABC blotting.

RESULTS

Reagents and procedures for nonradioactive, ultrasensitive site-specific protein–protein photocrosslinking

In previous work, we have developed reagents and procedures that enable identification of protein(s) and amino acid(s) close to a single, defined site of interest within a multiprotein complex by use of photocrosslinking and label transfer (19,20). The approach entails three steps (Figure 1A). In the first step, one prepares a multiprotein complex having a radiolabeled, cleavable photoactivatible crosslinking agent incorporated at a single, defined site of interest (Figure 1A, top; Figure 1B). In the second step, one photoirradiates the multiprotein complex initiating crosslinking (Figure 1A, center). In the third step, one cleaves the resulting crosslink(s), transferring radiolabel to the protein(s) and amino acid(s) at which crosslinking occurred, and one identifies the radiolabeled protein(s) and amino acid(s) (Figure 1A, bottom). The approach has been applied to analysis of protein–protein interactions within both bacterial transcription complexes (19,30) and eukaryotic transcription complexes (31–35). The approach is effective. However, the approach requires use of a radiolabel (^{125}I), and the approach has relatively low detection sensitivity [~2 fmol; limited by the maximum specific activity of ^{125}I (4.7 dpm/fmol) and the minimum activity of ^{125}I required to produce a distinct band in autoradiography (~10 dpm)].

In this work, we have developed reagents and procedures that enable nonradioactive, ultrasensitive identification of protein(s) and amino acid(s) close to a single, defined site of interest within a multiprotein complex by use of photocrosslinking and label transfer. The reagents and procedures are analogous to those of our previous work, except that the label is biotin (Figure 1B–D), the method of label detection is ABC blotting (Figure S1) and the formation, photoirradiation and processing of multiprotein complexes are performed on DNA fragments immobilized on agarose beads. Use of biotin as the label enables nonradioactive reagents. Use of ABC blotting as the method of label detection enables attamole-level detection sensitivity (~2 amol; representing a 1000-fold improvement over our previous work; Figure S1). Use of DNA fragments immobilized on agarose beads facilitates handling.

We have synthesized two biotin-labeled, cleavable photoactivatible crosslinking agents: B-AET (**III**; Figure 1C) and B-TEG-AET (**VI**; Figure 1D). The azidosalicylamido moiety present in each agent permits photocrosslinking. The 2-thiopyridyl moiety present in each agent permits cysteine-specific incorporation into a protein through a disulfide linkage—a linkage that can be cleaved quantitatively by treatment with dithiothreitol or 2-mercaptoethanol (Figure 1C and D). Each agent can be incorporated at a single, defined site within a protein by a two-step procedure consisting of: (i) site-directed mutagenesis to introduce a unique surface cysteine residue at the site of interest, followed by (ii) cysteine-specific chemical modification. For each agent, in the resulting derivatized protein, the length of the linker arm between the α carbon of the cysteine residue and the photoreactive atom is 14 Å (1.9 times the length of an arginine-side chain). The length of the linker arm is suitable for analysis of interactions occurring at, or just beyond, side-chain contact distance.

Both B-AET and B-TEG-AET are compatible with nonradioactive, ultrasensitive photocrosslinking and label transfer (Figures 2 and 3). B-TEG-AET offers an important additional advantage that, in proteins derivatized with this agent, the disulfide linkage between protein and probe is resistant to cleavage by low to moderate concentrations of 2-mercaptoethanol—presumably because the triethyleneglycol (TEG) linker hinders access by low to moderate concentrations of 2-mercaptothanol (Figure S2). As a result, proteins derivatized with this agent can be used in crosslinking reactions in the presence of low to moderate concentrations of 2-mercaptoethanol, and thus can be used in crosslinking reactions with multiprotein complexes, such as human RNAPII transcription initiation complexes (Y.K., D.R. and R.H.E., unpublished data), that undergo oxidative damage in the absence of reducing agents (Figure 3).

B-AET and B-TEG-AET bear similarities to biotin-labeled, cleavable photoactivatible crosslinking agents reported by Benkovic and co-workers (36–39) and Outten and co-workers (40). However, the agents reported by Benkovic and co-workers and Outten and co-workers yield derivatized proteins with longer linker arms between the α carbon of the cysteine residue and the photoreactive atom (18 Å versus 14 Å for B-AET and B-TEG-AET), rendering these agents less suitable for analysis of interactions occurring at, or just beyond, side-chain contact distance. In addition, to our knowledge, these agents have not been demonstrated to enable crosslinking with attamole-level detection sensitivity or to enable crosslinking reactions in the presence of low to moderate concentrations of 2-mercaptoethanol.

TBP derivatives for nonradioactive, ultrasensitive site-specific protein–protein photocrosslinking

We prepared a human TBPc derivative containing no solvent-accessible, reactive cysteine residues ([Thr176]TBPc,

(photocrosslinking agent of this work; detectable label is biotin). First line, synthesis. Second line, reaction with a protein having a unique surface cysteine residue to yield a conjugate of form [*S*-(2-((*N*-biotinyl-2-aminoethyl)carbamoyl)-2′-(4-azidosalicylamido)ethylthio)Cys]protein ([(B-AE)Cys]protein). In the resulting conjugate, the length of the linker arm between the α carbon of the cysteine residue and the photoreactive atom is 14 Å. (**D**) B-TEG-AET (photocrosslinking agent of this work; detectable label is biotin). First line, synthesis. Second line, reaction with a protein having a unique surface cysteine residue to yield a conjugate of form [*S*-(2-((*N*-biotinyl-11-amino-3,6,9-trioxaundecanyl)carbamoyl)-2′-(4-azidosalicylamido)ethylthio)Cys]protein ([(B-TEG-AE)Cys]protein). In the resulting conjugate, the length of the linker arm between the α carbon of the cysteine residue and the photoreactive atom is 14 Å.

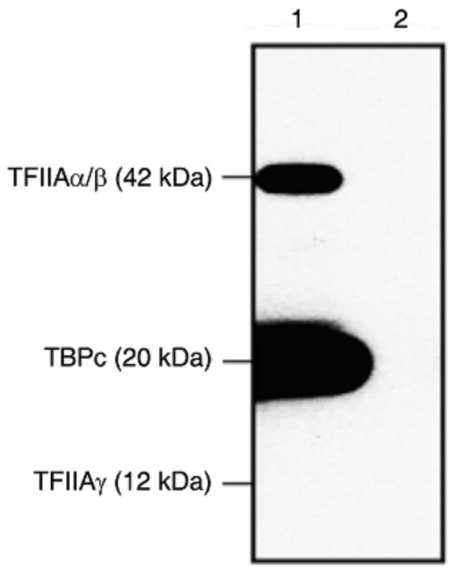

Figure 2. Site-specific protein–protein photocrosslinking between TBP H2 and TFIIA: crosslinking within the TFIIA–TBP–DNA complex. Biotin-labeled products of photocrosslinking followed by crosslink cleavage and label transfer (ABC blot of SDS–polyacrylamide gel). Lane 1, photocrosslinking reaction with TFIIA-[Thr176;(B-AE)Cys236]TBPc–DNA complex; lane 2, control reaction omitting UV-irradiation. Biotin-labeled TBPc is the product of intramolecular self-crosslinking; biotin-labeled TFIIAα/β is the product of intermolecular, TBPc → TFIIAα/β, crosslinking. Control experiments in the absence of DNA or in the absence of TFIIA show biotin-labeled TBPc but do not show biotin-labeled TFIIAα/β.

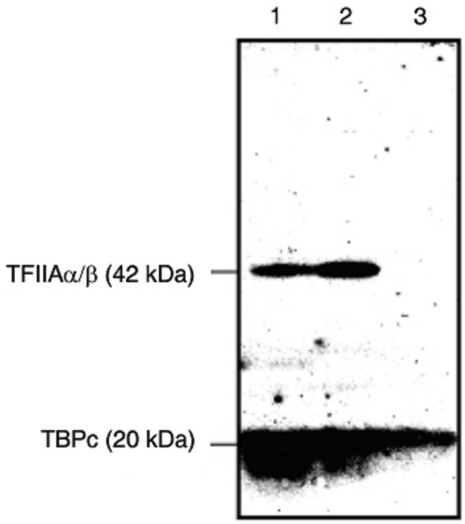

Figure 3. Site-specific protein–protein photocrosslinking between TBP H2 and TFIIA: crosslinking within the RNAPII–TFIIF–TFIIB–TFIIA–TBP–DNA complex. Biotin-labeled products of photocrosslinking followed by crosslink cleavage and label transfer (ABC blot of SDS–polyacrylamide gel). Lane 1, photocrosslinking reaction with RNAPII–TFIIF–TFIIB–TFIIA-[Thr176;(B-TEG-AE)Cys236]TBPc–DNA complex; lane 2, photocrosslinking reaction with TFIIA-[Thr176;(B-TEG-AE)Cys236]TBPc–DNA complex; lane 3, photocrosslinking reaction with [Thr176;(B-TEG-AE)Cys236]TBPc–DNA complex. Biotin-labeled TBPc is the product of intramolecular self-crosslinking; biotin-labeled TFIIAα/β is the product of intermolecular, TBPc → TFIIAα/β, crosslinking. Control experiments in the absence of DNA or in the absence of TFIIA show biotin-labeled TBPc but do not show biotin-labeled TFIIAα/β.

Figure S3) and a human TBPc derivative containing a unique solvent-accessible, reactive cysteine residue at position 236 ([Thr176;Cys236]TBPc; Figure S3), a position that is located within TBP H2 but that is not essential for TFIIA–TBP or NC2-TBP interactions [(15); Y.K., D.R. and R.H.E., unpublished data]. [Wild-type human TBPc contains a single solvent-accessible, reactive cysteine residue: i.e. Cys176 (Figure S3). Substitution of Cys176 by Thr yields a TBPc derivative containing no solvent-accessible, reactive cysteine residues (Figure S3), and further substitution of Arg236 by Cys yields a TBPc derivative having a single solvent-accessible, reactive cysteine residue: i.e. Cys236 (Figure S3).] We reacted [Thr176;Cys236]TBPc with B-AET, yielding a human TBPc derivative containing a biotin-labeled, cleavable photoactivatible crosslinking agent site-specifically incorporated at position 236 within TBP H2 ([Thr176;(B-AE)Cys236]TBPc; Figures 1D, S4 and S5). The efficiency of incorporation was ≥95% (as assessed spectrophotometrically; Figure S4), and the site-specificity of incorporation was ≥95% (as assessed spectrophotometrically in parallel reactions with [Thr176]TBPc; Figure S4). The resulting TBPc derivative was fully functional in formation of TFIIA–TBP–DNA and NC2–TBP–DNA complexes (Figure S5). In the resulting TBPc derivative, the disulfide linkage between protein and probe was quantitatively cleaved by 2-mercaptoethanol at concentrations of ≥0.8 mM (reactions for 30 min at 30°C; Figure S2).

In the same manner, we reacted [Thr176;Cys236]TBPc with B-TEG-AET, yielding a second biotin-labeled, cleavable photoactivatible crosslinking agent site-specifically incorporated at position 236 within TBP H2 ([Thr176;(B-TEG-AE)Cys236]TBPc; Figures 1D, S6, S7). The efficiency of incorporation was ≥95% (as assessed spectrophotometrically; Figure S6), and the site specificity of incorporation was ≥95% (as assessed spectrophotometrically in parallel reactions with [Thr176]TBPc; Figure S6). The resulting TBPc derivative was fully functional in formation of TFIIA–TBP–DNA and RNAPII–TFIIF–TFIIB–TFIIA–TBP–DNA complexes (Figure S7). In the resulting TBPc derivative, the disulfide linkage between protein and probe was quantitatively cleaved by 2-mercaptoethanol at concentrations of ≥10 mM, but was substantially resistant to cleavage by 2-mercaptoethanol at a concentration of 1 mM and was partly resistant to cleavage by 2-mercaptoethanol at a concentration of 5 mM (reactions for 30 min at 30°C; Figure S2).

Site-specific protein–protein photocrosslinking between TBP H2 and TFIIA: crosslinking within the TFIIA–TBP–DNA complex

To assess interactions between human TFIIA and human TBP H2 within the TFIIA-TBP–DNA complex in solution, we performed site-specific protein–protein photocrosslinking using [Thr176;(B-AE)Cys236]TBPc. The results are presented in Figure 2. The results indicate that crosslinking between TFIIA and TBP H2 occurs and is efficient (with an efficiency ~20% of the efficiency of intramolecular, self-crosslinking). The results further indicate that crosslinking occurs exclusively with the

TFIIA α/β subunit (with no detectable crosslinking to the TFII γ subunit). Control experiments establish that crosslinking requires UV-irradiation, TFIIA and DNA. We conclude that human TFIIAα/β is in direct physical proximity to human TBP H2 within the TFIIA–TBP–DNA complex in solution.

Site-specific protein–protein photocrosslinking between TBP H2 and TFIIA: crosslinking within the RNAPII–TFIIF–TFIIB–TFIIA–TBP–DNA complex

To determine whether interactions between human TFIIAα/β and human TBP H2 also occur in a higher order transcription–initiation complex, the RNAPII–TFIIF–TFIIB–TFIIA–TBP–DNA complex, we performed site-specific protein–protein photocrosslinking using [Thr176;(B-TEG-AE)Cys236]TBPc. [The disulfide linkage between protein and probe in [Thr176;(B-AE)Cys236]TBPc is cleaved by low to moderate concentrations of reducing agents (Figure S2); therefore, this TBPc derivative is not suitable for crosslinking experiments involving human RNAPII, which undergoes rapid oxidative damage and rapid loss of activity, in the absence of reducing agents (Y.K., D.R. and R.H.E., unpublished data). In contrast, the disulfide linkage between protein and probe in [Thr176;(B-TEG-AE)Cys236]TBPc is resistant to cleavage by low to moderate concentrations of 2-mercaptoethanol (presumably because the TEG linker hinders access by 2-mercaptoethanol; Figure S2); therefore, this TBPc derivative is suitable for crosslinking experiments involving human RNAPII.] The results are presented in Figure 3. The results indicate that crosslinking between TFIIA and TBP H2 occurs and is efficient (with an efficiency ~20–30% of the efficiency of intramolecular, self-crosslinking). The results further indicate that crosslinking occurs essentially exclusively with the TFIIA α/β subunit. There is no significant crosslinking to TFIIγ, TFIIB, TFIIF subunits or to RNAPII subunits [all of which are electrophoretically well resolved from TFIIAα/β; see Ref. (26)]. Control experiments establish that crosslinking requires UV-irradiation, TFIIA and DNA. Further control experiments establish that, under the reaction conditions used, [Thr176;(B-TEG-AE)Cys236]TBPc yields RNAPII–TFIIF–TFIIB–TFIIA–TBP–DNA complexes and does not yield TFIIA–TBP–DNA subcomplexes, implying that the observed crosslinking arises from RNAPII–TFIIF–TFIIB-TFIIA-TBP-DNA complexes and not from TFIIA–TBP–DNA subcomplexes (Figure S7). We conclude that TFIIAα/β is in direct physical proximity to human TBP H2 within the RNAPII-TFIIF–TFIIB–TFIIA–TBP–DNA complex in solution.

Site-specific protein–protein photocrosslinking between TBP H2 and TFIIA: mapping of crosslinks in TFIIAα/β

To define the site(s) on human TFIIAα/β at which crosslinking occurs, we performed cysteine-specific proteolytic mapping with 2-nitro-5-thiocyanatobenzoic acid (41). We performed parallel reactions with wild-type TFIIA, which contains a single cysteine residue at TFIIα/β position 337, and with TFIIA derivatives—each verified to be functional in formation of, and crosslinking within, the TFIIA-TBP-DNA complex (Figure S8)—containing engineered single cysteine residues at TFIIAα/β positions 61, 135, 214 and 280 (Figure 4A). [Wild-type human TFIIAα/β contains a single cysteine residue: i.e. Cys337 (Figure 4A). Substitution of Cys337 by Ala yields a TFIIAα/β derivative containing no cysteine residues (Figure 4A), and further substitution of residues Ser61, Ser135, Ser214 and Ser280 by Cys yields a set of four TFIIAα/β derivatives each having a single cysteine residue: i.e. Cys61, Cys135, Cys214 and Cys280 (Figure 4A).] The results are presented in Figure 4B–C. The results indicate that crosslinking occurs essentially exclusively within residues 61–134 of TFIIAα/β. These residues are located within the 'connector' segment of TFIIAα/β, between the α-homologous and β-homologous segments of TFIIAα/β (Figure 4A). They comprise the N-terminal third of the 'connector' segment of TFIIAα/β (Figure 4A). We conclude that the N-terminal third of the 'connector' segment of human TFIIAα/β is in direct physical proximity to human TBP H2 within the TFIIA–TBP–DNA complex in solution.

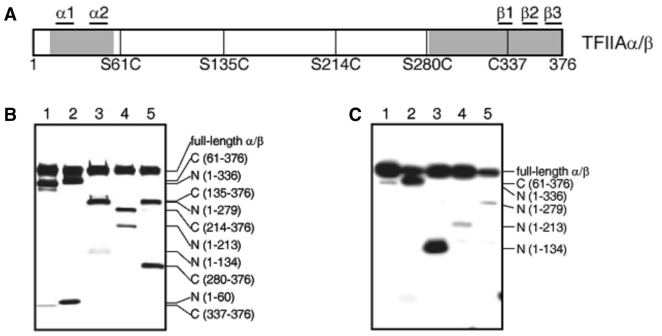

Figure 4. Site-specific protein–protein photocrosslinking between TBP H2 and TFIIA: mapping of crosslinks in TFIIAα/β. (**A**) Positions of Cys residues in engineered single-Cys TFIIAα/β derivatives. The TFIIAα domain and TFIIAβ domain are indicated by shading; α-helices and β-strands are numbered. (**B**) Products of Cys-specific cleavage of engineered single-Cys TFIIAα/β derivatives (silver-stained SDS–polyacrylamide gel). Product identities are based on results of blotting with Ni^{2+}-NTA-conjugated horseradish peroxidase, which detects products containing the heptahistidine sequence at TFIIAα/β positions 81–87 (Figure S9). (**C**) Biotin-labeled products of formation of TFIIA-[Thr176;(B-AE)Cys236]TBPc–DNA complex with engineered single-Cys TFIIAα/β derivatives, photocrosslinking, crosslink cleavage, label transfer and Cys-specific cleavage (ABC blot of SDS–polyacrylamide gel).

Site-specific protein–protein photocrosslinking between TBP H2 and NC2: crosslinking within the NC2-TBP-DNA complex

To assess interactions between human NC2 and human TBP H2 within the NC2-TBP-DNA complex in solution, we performed site-specific protein–protein photocrosslinking using [Thr176;(B-AE)Cys236]TBPc. The results are presented in Figure 5. The results indicate that crosslinking between NC2 and TBP H2 occurs and is efficient (with an efficiency ~10% of the efficiency of intramolecular, self-crosslinking). The results further indicate that crosslinking occurs exclusively with the NC2 α subunit (with no detectable crosslinking to the NC2 β

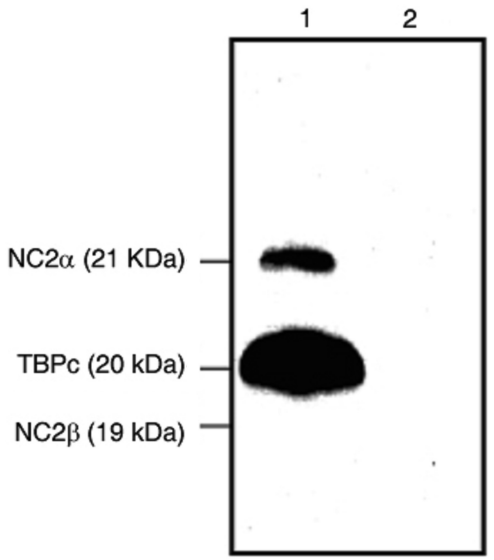

Figure 5. Site-specific protein–protein photocrosslinking between TBP H2 and NC2: crosslinking within the NC2–TBP–DNA complex. Biotin-labeled products of photocrosslinking followed by crosslink cleavage and label transfer (ABC blot of SDS–polyacrylamide gel). Lane 1, photocrosslinking reaction with NC2–[Thr176;(B-AE)Cys236]TBPc–DNA complex; lane 2, control reaction omitting UV-irradiation. Biotin-labeled TBPc is the product of intramolecular self-crosslinking; biotin-labeled NC2α is the product of intermolecular, TBPc → NC2α, crosslinking. Control experiments in the absence of DNA or in the absence of NC2 show biotin-labeled TBPc but do not show biotin-labeled NC2α.

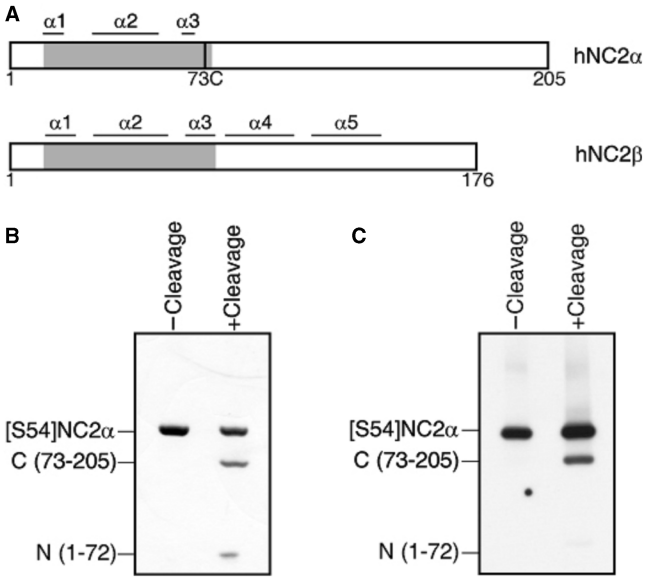

Figure 6. Site-specific protein–protein photocrosslinking between TBP H2 and NC2: mapping of crosslinks in NC2α. (**A**) Position of the Cys residue in the engineered single-Cys NC2α derivative. Histone-fold domains are indicated by shading; α-helices are numbered. (**B**) Products of Cys-specific cleavage of the engineered single-Cys NC2α derivative (silver-stained SDS–polyacrylamide gel). (**C**) Biotin-labeled products of formation of NC2–[Thr176;(B-AE)Cys236]TBPc–DNA complex with the engineered single-Cys NC2α derivative, photocrosslinking, crosslink cleavage, label transfer and Cys-specific cleavage (ABC blot of SDS–polyacrylamide gel).

subunit). Control experiments establish that crosslinking requires UV-irradiation, NC2 and DNA. We conclude that human NC2α is in direct physical proximity to human TBP H2 within the NC2-TBP-DNA complex in solution.

Site-specific protein–protein photocrosslinking between TBP H2 and NC2: mapping of crosslinks in NC2α

To define the site(s) on human NC2α at which crosslinking occurs, we performed cysteine-specific proteolytic mapping with 2-nitro-5-thiocyanatobenzoic acid (41). We performed reactions with an NC2 derivative—verified to be functional in formation of, and crosslinking within, the NC2-TBP-DNA complex (Figure S10)—containing an engineered single cysteine residue at position 73. [Wild-type human NC2α contains two cysteine residues: i.e. Cys54 and Cys73; substitution of Cys54 by Ser yields an NC2α derivative containing a single cysteine residue: i.e. Cys73 (Figure 6A).] This position is located at the boundary between the N-terminal histone-fold domain of NC2α and the C-terminal 'tail' of NC2α (Figure 6A). The results are presented in Figure 6B and C. The results indicate that crosslinking occurs essentially exclusively within the segment containing residues 73–205 of NC2α, and thus that crosslinking occurs essentially exclusively within the segment corresponding to the C-terminal 'tail' of NC2α. We conclude that the C-terminal 'tail' segment of human NC2α is in direct physical proximity to human TBP H2 within the NC2-TBP-DNA complex in solution.

DISCUSSION

Nonradioactive, ultrasensitive site-specific protein–protein photocrosslinking

We have extended our previous approach for site-specific protein–protein photocrosslinking (19,20) by providing reagents and procedures for nonradioactive, ultrasensitive site-specific protein–protein photocrosslinking (Figures 1, S1). The reagents and procedures permit a detection sensitivity of ~2 amol (a 1000-fold improvement in detection sensitivity over our previous work), enabling application of the approach to multiprotein complexes, such as human RNAPII-containing transcription complexes, that are difficult to prepare in large quantities. One of the reagents, B-TEG-AET, permits crosslinking in the presence of 2-mercaptoethanol at concentrations up to ~5 mM (Figure S2), enabling application of the approach to multiprotein complexes, such as human RNAPII-containing transcription complexes, that are unstable in the absence of reducing agents. The reagents and procedures are generalizable. In this work, we have applied the reagents and procedures to analysis of TFIIA-TBP interactions in the human TFIIA–TBP–DNA and RNAPII–TFIIF–TFIIB–TFIIA–TBP–DNA complexes and to analysis of NC2-TBP interactions in the human NC2–TBP–DNA complex (Figures 2–6). In other work, we have applied the reagents and procedures to analysis of TFIIB–TBP interactions in the human TFIIB–TBP–DNA, RNAPII–TFIIF–TFIIB–TBP–DNA and RNAPII–TFIIF–TFIIB–TFIIA–TBP–DNA complexes (Y.K., Y.W.E, D.R. and R.H.E., unpublished data). In still other work, we

have applied the reagents and procedures to static and kinetic analysis of CAP-RNAP interactions in bacterial CAP–RNAP-DNA complexes (Druzhinin, S., Y.K., Y.W.E. and R.H.E., unpublished data).

TFIIA–TBP interaction: the TFIIAα/β 'connector' interacts with TBP H2

Our results indicate that the 'connector' segment of human TFIIA α/β subunit is in direct physical proximity to H2 of human TBP in the TFIIA–TBP–DNA complex in solution and in the RNAPII–TFIIF–TFIIB–TFIIA–TBP–DNA complex in solution. The contact or close approach involves amino acids 61–134 of human TFIIAα/β subunit, which correspond to, but do not show obvious amino acid sequence similarity to, amino acids 57–131 of yeast TFIIA TOA1 subunit.

A contact or close approach between residues 61–134 of the TFIIAα/β connector and TBP H2 was not observed in published crystal structures of TFIIA–TBP–DNA complexes, since most (in one crystal structure), or all (in three crystal structures), of these residues were omitted from the truncated TFIIA derivatives used in crystallization (8–10). Nevertheless, a contact or close approach between these residues of the TFIIAα/β connector and TBP H2 would be compatible with published crystal structures of TFIIA–TBP–DNA complexes, based on the locations of residues preceding and following the connector, and on the accessibility and location of TBP H2 (which is prominently exposed on the face of TBP closest to TFIIA).

We propose that residues 61–134 of the human TFIIAα/β connector make functional interactions with TBP H2—interacting directly with TBP H2 and/or buttressing and positioning residues that interact directly with TBP H2—and we propose that these functional interactions account for genetic and NMR-spectroscopic evidence suggesting involvement of TBP H2 in TFIIA–TBP interaction (12–17).

NC2–TBP interaction: the NC2α C-terminal 'tail' interacts with TBP H2

Our results indicate that the C-terminal 'tail' of human NC2α subunit—the segment of NC2α following the histone-fold core domain of NC2α—is in direct physical proximity to H2 of human TBP in the NC2-TBP-DNA complex in solution. The contact or close approach involves amino acids 73–205 of human NC2α subunit, which correspond to, and which contain a segment with obvious amino acid sequence similarity to, amino acids 114–142 of yeast NC2α subunit.

A contact or close approach between residues the NC2α C-terminal tail and TBP H2 was not observed in the published crystal structure of a NC2–TBP–DNA complex, since the C-terminal tail was omitted, essentially in its entirety, from the truncated NC2α derivative used in crystallization (7). Nevertheless, a contact or close approach between the NC2α C-terminal tail and TBP H2 would be compatible with the published crystal structure, based on the accessibility and location of the C-terminal residue of the truncated NC2α derivative (which is prominently exposed on the face of NC2 closest to TBP H2) and on the accessibility and location of TBP H2 (which is prominently exposed on the face of TBP closest to NC2α).

We propose that the human NC2α C-terminal tail makes direct, functional interactions with TBP H2, and we propose that these direct, functional interactions account for genetic evidence suggesting involvement of the NC2α C-terminal tail in NC2–TBP interaction and NC2-dependent transcriptional repression (42,43) and for genetic evidence suggesting involvement of TBP H2 in NC2–TBP interaction (18).

NC2–TFIIA competition

Comparison of published crystal structures of NC2–TBP–DNA and TFIIA–TBP–DNA complexes does not provide an obvious structural basis for competition between NC2 and TFIIA for interactions with the TBP–DNA complex (7–10). There is minimal overlap, and minimal steric incompatibility, between positions of residues of NC2 and TFIIA that interact with TBP, and there is no overlap, and no steric incompatibility, between residues of NC2 and TFIIA that interact with DNA.

Our finding that the TFIIA and NC2—segments that had been omitted from the truncated TFIIA and NC2 derivatives used in crystallization—interact with H2 of TBP provides a simple structural basis for competition between NC2 and TFIIA. Our findings suggest that competition between NC2 and TFIIA involves overlap, and steric incompatibility, between positions of residues of the NC2α C-terminal tail that interact with TBP H2 and positions of residues of the TFIIAα/β connector that interact with TBP H2.

Previous results indicate that NC2β subunit functions in repression by using a C-terminal tail to interact with, and to mask, a surface of TBP that alternatively interacts with the general transcription factor TFIIB (7). Here, we propose that NC2α subunit functions in repression through an analogous mechanism: using a C-terminal tail to interact with, and to mask, a surface of TBP that alternatively interacts with the general transcription factor TFIIA. Thus, we propose that NC2 employs two analogous, but independent, mechanisms to target TBP, each mediated by the C-terminal tail of an NC2 subunit.

SUPPLEMENTARY DATA

Supplementary Data are available at NAR Online.

ACKNOWLEDGEMENT

We thank Paul Lieberman for plasmids and for discussion.

FUNDING

National Institutes of Health (GM51527 to R.H.E.); Howard Hughes Medical Institute (Investigatorship to R.H.E., Investigatorship to D.R.). Funding for the open access charge: Howard Hughes Medical Institute.

Conflict of interest statement. None declared.

REFERENCES

1. Burley,S. and Roeder,R. (1996) Biochemistry and structural biology of transcription factor IID (TFIID). *Ann. Rev. Biochem.*, **65**, 769–799.
2. Orphanides,G., Lagrange,T. and Reinberg,D. (1996) The general transcription factors of RNA polymerase II. *Genes Dev.*, **10**, 2657–2683.
3. Woychik,N. and Hampsey,M. (2002) The RNA polymerase II machinery: structure illuminates function. *Cell*, **108**, 453–463.
4. Hahn,S. (2004) Structure and mechanism of the RNA polymerase II transcription machinery. *Nat. Struct. Mol. Biol.*, **11**, 394–403.
5. Høiby,T., Zhou,H., Mitsiou,D. and Stunnenberg,H. (2007) A facelift for the general transcription factor TFIIA. *Biochim. Biophys. Acta*, **1769**, 429–436.
6. Kaiser,K. and Meisterernst,M. (1996) The human general co-factors. *Trends Biochem. Sci.*, **21**, 342–345.
7. Kamada,K., Shu,F., Chen,H., Malik,S., Stelzer,G., Roeder,R., Meisterernst,M. and Burley,S. (2001) Crystal structure of negative cofactor 2 recognizing the TBP-DNA transcription complex. *Cell*, **106**, 71–81.
8. Geiger,J., Hahn,S., Lee,S. and Sigler,P. (1996) Crystal structure of the yeast TFIIA/TBP/DNA complex. *Science*, **272**, 830–836.
9. Tan,S., Hunziker,Y., Sargent,D. and Richmond,T. (1996) Crystal structure of a yeast TFIIA/TBP/DNA complex. *Nature*, **381**, 127–134.
10. Bleichenbacher,M., Tan,S. and Richmond,T. (2003) Novel interactions between the components of human and yeast TFIIA/TBP/DNA complexes. *J. Mol. Biol.*, **332**, 783–793.
11. Bryant,G., Martel,L., Burley,S. and Berk,A. (1996) Radical mutations reveal TATA-box binding protein surfaces required for activated transcription in vivo. *Genes Dev.*, **10**, 2491–2504.
12. Lee,D.K., Dejong,J., Hashimoto,S., Horikoshi,M. and Roeder,R. (1992) TFIIA induces conformational change in TFIID via interactions with the basic repeat. *Mol. Cell Biol.*, **12**, 5189–5196.
13. Buratowski,S. and Zhou,H. (1992) Transcription factor IID mutants defective for interaction with transcription factor IIA. *Science*, **255**, 1130–1132.
14. Stargell,L. and Struhl,K. (1995) The TBP-TFIIA interaction in the response to acidic activators in vivo. *Science*, **269**, 75–78.
15. Tang,H., Sun,X., Reinberg,D. and Ebright,R.H. (1996) Protein-protein interactions in eukaryotic transcription initiation: structure of the pre-initiation complex. *Proc. Natl Acad. Sci. USA*, **93**, 1119–1124.
16. Cang,Y., Auble,D. and Prelich,G. (1999) A new regulatory domain on the TATA-binding protein. *EMBO J.*, **18**, 6662–6671.
17. Bagby,S., Mal,T., Liu,D., Raddatz,E., Nakatani,Y. and Ikura,M. (2000) TFIIA-TAF regulatory interplay: NMR evidence for overlapping binding sites on TBP. *FEBS Lett.*, **468**, 149–154.
18. Kim,T.K., Zhao,Y., Ge,H., Bernstein,R. and Roeder,R. (1995) TATA-binding protein residues implicated in a functional interplay between negative cofactor NC2 (DR1) and general factors TFIIA and TFIIB. *J. Biol. Chem.*, **270**, 10976–10981.
19. Chen,Y., Ebright,Y. and Ebright,R. (1994) Identification of the target of a transcription activator protein by protein-protein photocrosslinking. *Science*, **265**, 90–92.
20. Ebright,Y., Chen,Y., Kim,Y. and Ebright,R. (1996) S-[2-(4-azidosalicylamido)ethanethio]-2-thiopyridine: radioiodinatable, cleavable photoactivatible crosslinking agent. *Bioconj. Chem.*, **7**, 380–384.
21. Kunkel,T., Bebenek,K. and McClary,J. (1991) Efficient site-directed mutagenesis using uracil-containing DNA. *Methods Enzymol.*, **204**, 125–138.
22. Ellman,G. (1959) Tissue sulfhydryl groups. *Arch. Biochem. Biophys.*, **82**, 70–77.
23. Ozer,J., Moore,P., Bolden,A., Lee,A., Rosen,C. and Lieberman,P. (1994) Molecular cloning of the small (gamma) subunit of human TFIIA reveals functions critical for activated transcription. *Genes Dev.*, **8**, 2324–2335.
24. Mermelstein,F., Yeung,K., Cao,J., Inostroza,J., Erdjument-Bromage,H., Eagelson,K., Landsman,D., Levitt,P., Tempst,P. and Reinberg,D. (1996) Requirement of a corepressor for Dr1-mediated repression of transcription. *Genes Dev.*, **10**, 1033–1048.
25. White,R., Khoo,B., Inostroza,J., Reinberg,D. and Jackson,S. (1994) Differential regulation of RNA polymerases I, II, and III by the TBP-binding repressor Dr1. *Science*, **266**, 448–450.
26. Maldonado,E., Drapkin,R. and Reinberg,D. (1996) Purification of human RNA polymerase II and general transcription factors. *Methods. Enzymol.*, **274**, 72–100.
27. Laemmli,U. (1970) Cleavage of structural proteins during the assembly of the head of bacteriophage T4. *Nature*, **227**, 680–685.
28. Hudgin,R., Pricer,W., Ashwell,G., Stockert,R. and Morell,A. (1974) The isolation and properties of a rabbit liver binding protein specific for asialoglycoproteins. *J. Biol. Chem.*, **249**, 5536–5543.
29. Hager,D. and Burgess,R. (1980) Elution of proteins from sodium dodecyl sulfate-polyacrylamide gels, removal of sodium dodecyl sulfate, and renaturation of enzymatic activity. *Anal. Biochem.*, **109**, 76–86.
30. Niu,W., Kim,Y., Tau,G., Heyduk,T. and Ebright,R. (1996) Transcription activation at Class II CAP-dependent promoters: two interactions between CAP and RNA polymerase. *Cell*, **87**, 1123–1134.
31. Ansari,A., Koh,S.S., Zaman,Z., Bongards,C., Lehming,N., Young,R. and Ptashne,M. (2002) Transcriptional activating regions target a cyclin-dependent kinase. *Proc. Natl Acad. Sci. USA*, **99**, 14706–14709.
32. Chen,H. and Hahn,S. (2004) Mapping the location of TFIIB within the RNA polymerase II transcription preinitiation complex: a model for the structure of the PIC. *Cell*, **119**, 169–180.
33. Warfield,L., Ranish,J. and Hahn,S. (2004) Positive and negative functions of the SAGA complex mediated through interaction of Spt8 with TBP and the N-terminal domain of TFIIA. *Genes Dev.*, **18**, 1022–1034.
34. Reeves,W. and Hahn,S. (2005) Targets of the Gal4 transcription activator in functional transcription complexes. *Mol. Cell Biol.*, **25**, 9092–9102.
35. Fishburn,J., Mohibullah,N. and Hahn,S. (2005) Function of a eukaryotic transcription activator during the transcription cycle. *Mol. Cell*, **18**, 369–378.
36. Alley,S., Ishmael,F., Daniel Jones,A. and Benkovic,S. (2000) Mapping protein-protein interactions in the bacteriophage T4 DNA polymerase holoenzyme using a novel trifunctional photocross-linking and affinity reagent. *J. Am. Chem. Soc.*, **122**, 6126–6127.
37. Ishmael,F., Alley,S. and Benkovic,S. (2001) Identification and mapping of protein-protein interactions between gp32 and gp59 by cross-linking. *J. Biol. Chem.*, **276**, 25236–25242.
38. Ishmael,F., Alley,S. and Benkovic,S. (2002) Assembly of the bacteriophage T4 helicase: architecture and stoichiometry of the gp41-gp59 complex. *J. Biol. Chem.*, **277**, 20555–20562.
39. Ishmael,F., Trakselis,M. and Benkovic,S. (2003) Protein-protein interactions in the bacteriophage T4 replisome. The leading strand holoenzyme is physically linked to the lagging strand holoenzyme and the primosome. *J. Biol. Chem.*, **278**, 3145–3152.
40. Layer,G., Gaddam,S., Ayala-Castro,C., Ollagnier-de Choudens,S., Lascoux,D., Fontecave,M. and Outten,F. (2007) SufE transfers sulfur from SufS to SufB for iron-sulfur cluster assembly. *J. Biol. Chem.*, **282**, 13342–13350.
41. Jacobson,J., Schaffer,M., Stark,G. and Vanaman,T. (1973) Specific chemical cleavage in high yield at the amino peptide bonds of cysteine and cystine residues. *J. Biol. Chem.*, **248**, 6583–6591.
42. Goppelt,A., Stelzer,G., Lottspeich,F. and Meisterernst,M. (1996) A mechanism for repression of class II gene transcription through specific binding of NC2 to TBP-promoter complexes via heterodimeric histone fold domains. *EMBO J.*, **15**, 3105–3116.
43. Gilfillan,S., Stelzer,G., Piaia,E., Hofmann,M. and Meisterernst,M. (2005) Efficient binding of NC2·TATA-binding protein to DNA in the absence of TATA. *J. Biol. Chem.*, **280**, 6222–6230.